Chemical Engineering Journal 102 (2004) 131–140

Chemical Engineering Journal

www.elsevier.com/locate/cej

Mass transfer at gas sparged interface between two immiscible nondispersed liquids in batch and continuous reactors

A.H. Konsowa, M.S. Abdo, M.S. Hassan, G.H. Sedahmed*

Chemical Engineering Department, Faculty of Engineering, Alexandria University, Alexandria, Egypt

Received 8 August 2003; accepted 13 March 2004

Abstract

Mass transfer between gas sparged two immiscible nondispersed liquids was studied by measuring the limiting current of the cathodic reduction of ferricyanide ion at the surface of a mercury pool cathode. Rates of mass transfer were measured for three cases, namely: (i) batch gas sparged reactor; (ii) continuous gas sparged reactor with superimposed solution flow admitted to the reactor from a side entry nozzle located at the mercury surface; (iii) continuous single phase flow reactor (unsparged). Variables studied were N_2 superficial velocity, physical properties of the solution, solution velocity and inlet nozzle diameter (d_n). The following correlations were obtained for solutions of *Sc* ranging from 1740 to 6000. Single phase mass transfer data without gas sparging were correlated by the equation:

$$Sh = 0.236\, Sc^{0.33}\, Re^{0.89} \left(\frac{d}{d_n}\right)^{0.68}$$

Gas sparging mass transfer data in a batch reactor were correlated in terms of the mass transfer *J* factor by the equation:

$$J = 0.39(Re\, Fr)^{-0.16}$$

Mass transfer data obtained for the combined gas sparging and single phase flow were found to fit the equation:

$$Sh = 28\, Sc^{0.33}\, Re^{0.24}\, Re_g^{0.28}$$

Implications of the present results for enhancing the rate of diffusion controlled chemical and metallurgical processes between two immiscible nondispersed liquids, and design of electrochemical reactors employing mercury pool cathode are noted.

Keywords: Liquid–liquid mass transfer; Gas sparging; Electrochemical reactors

1. Introduction

Gas sparging is assuming a growing importance as a means for intensifying diffusion controlled technical processes such as electrochemical processes [1–4], biochemical processes [5,6], membrane processes [7] and heterogeneous (liquid–solid, gas–liquid and liquid–liquid) and catalytic reactions [8–11]. The increasing acceptance of gas sparging by industry is attributed to: (i) for a given rate of mass transfer, gas sparging is more economic than mechanical stirring [10,12]; (ii) gas sparging can offer considerable advantages over mechanical stirring especially at high pressures where shaft sealing is a problem and in vessels of large length to diameter ratio where mechanical stirring is awkward to arrange.

So far, most of the previous mass transfer studies in gas sparged systems have concentrated on solid–liquid, gas–liquid and dispersed liquid–liquid systems. Scant attention has been given to the use of gas sparging to enhance the rate of heat and mass transfer between immiscible nondispersed liquid–liquid systems despite their frequent occurrence in chemical engineering practice as shown by the following examples:

(1) Liquid–liquid extraction with or without chemical reaction between liquids which are difficult to disperse either because of the large difference in properties between the two liquids (density, viscosity and surface tension) or when dispersion is undesirable owing to the formation of a difficult to break stable emulsion.

* Corresponding author.
E-mail address: konsowa2002@yahoo.com (G.H. Sedahmed).

1385-8947/$ – see front matter © 2004 Elsevier B.V. All rights reserved.
doi:10.1016/j.cej.2004.03.002

Nomenclature

a, $\breve{a}$	constants
A	projected cathode area
C	ferricyanide concentration
d	mercury pool diameter (reactor diameter)
d_b	bubble diameter
d_n	nozzle diameter
D	ferricyanide diffusivity
F	Faraday's constant
Fr	Froude number (V_g^2/dg)
g	acceleration due to gravity
J	mass transfer J factor ($St \times Sc^{0.66}$)
K	mass transfer coefficient due to single phase flow
$\bar{K}$	overall mass transfer coefficient
K_g	mass transfer coefficient due to gas sparging
l	limiting current
Q	volumetric flow rate of the solution
r_b	bubble radius
Re	solution Reynolds number ($\rho V d/\mu$)
Re_g	gas Reynolds number ($\rho V_g d/\mu$)
Re_n	nozzle Reynolds number ($\rho V d_n/\mu$)
Sc	Schmidt number (ν/D)
Sh	Sherwood number (Kd/D)
St	Stanton number (K_g/V)
t	time
T	temperature
V	solution velocity in the reactor ($Q/(\pi d^2/4)$)
V_b	bubble volume
V_g	superficial gas velocity
V_n	nozzle solution velocity
Z	number of electrons involved in the reaction

Greek letters

θ	fractional surface coverage by gas bubbles
μ	solution density
ν	kinematic viscosity
ρ_1, ρ_2, ρ_g	density of heavy liquid, light liquid and gas, respectively
σ	surface tension
ϕ	bubble shape factor

(2) Liquid–liquid extraction under high pressure using supercritical fluids (e.g. liquefied carbon dioxide) to separate isomers from organic melts [13].
(3) Metallurgical reactions where a layer of slag floats on a molten metal phase extracts a component from the molten metal solution [14].
(4) Pure mercury needed for applications such as thermometry and temperature control is produced from impure mercury by dissolving the less noble impurities in an oxidizing agent such as HNO_3 or $Hg(NO_3)_2$ which dissolves the less noble metal impurities from impure mercury and deposit an equivalent amount of mercury (cementation) [15,16].
(5) Liquid amalgams which are used as a strong reducing agents for reducing organic [17] and inorganic compounds [18] are produced electrochemically using a mercury pool cathode.
(6) Mercury pool cathode is used as an efficient cathode for electrochemical reduction of aqueous organic and inorganic compounds [19–22] which are difficult to reduce by other efficient solid cathodes such as Zn, Pb and Sn and solid amalgams. Examples of industrial small scale electroorganic synthesis using mercury as a cathode are mentioned elsewhere [20]. The high efficiency of mercury cathode is attributed to: (i) mercury has a high H_2 overpotential which may exceed 1 V, this makes it possible to reduce a wide range of organic compounds at the mercury surface in preference to H_2 evolution; (ii) mercury has a clean and reproducible surface unlike solid electrodes which may be deactivated during electrolysis by fouling organic deposits; (iii) mercury acts as a catalyst for the reduction of many organic compounds. The negative environmental effects of using mercury as cathode material have been reduced considerably by the advent of three-dimensional electrodes which could reduce the level of mercury ion concentration in waste solution to below the maximum permissible value [23,24]. On the other side the mercury pool cathode suffers from a limited area which limits its space time yield, this shortcoming can be overcome by enhancing the rate of mass transfer.

The aim of the present work is to test the effect of gas sparging on the rate of mass transfer between immiscible nondispersed liquids in batch and continuous reactors. To this end, the rate of mass transfer between a horizontal mercury pool cathode and an aqueous solution was determined by measuring the limiting current of the cathodic reduction of ferricyanide ion in a large excess of sodium hydroxide for following arrangements: (i) batch gas sparged reactor; (ii) continuous gas sparged reactor with superimposed solution flow fed to the reactor through a side entry nozzle located at the mercury surface; (iii) continuous single phase flow reactor without gas sparging.

Although theoretical and empirical equations are available in the literature to predict the rate of heat [25] and mass transfer [26–28] in gas sparged liquid–solid systems, little has been done to quantify the heat and mass transfer behaviour of two immiscible nondispersed liquids stirred by inert gas bubbles introduced from below the heavy liquid layer. In view of the analogy between heat and mass transfer, it is hoped that the present results could be transposed to heat transfer between immiscible nondispersed liquids. This would serve objects such as the thermal management of chemical and metallurgical processes involving two immiscible nondispersed liquids, and waste heat recovery from hot liquid metals such as mercury and gallium (melting point =

29 °C) by direct cooling with water in the production stage of these metals.

2. Theory

In view of the approximate similarity between bubble formation at the surface of gas sparged mercury layer and electrically generated gas bubbles at solid electrodes, mass transfer at gas sparged mercury pool can be dealt with approximately in a manner similar to mass transfer at gas evolving solid electrode using the following models:

(1) *The natural convection model* (*the macroconvection model*). This model was originally developed by Zuber [29] to explain the mechanism of heat transfer during nucleate boiling. The model was used to explain the mechanism of mass transfer at gas evolving electrodes [30,31]. This model is based on the fact that the difference in density between the liquid and the average density of the gas–liquid layer at the mercury surface gives rise to an upward buoyancy force which removes the reacted solution from the mercury surface and replaces it with a fresh bulk solution. Previous natural convection studies at an upward facing horizontal surface [32,33] lead to the equation:

$$Sh = a(Sc\,Gr)^{0.33} \tag{1}$$

where

$$Gr = \frac{gd_g^3}{\gamma^2}\frac{\Delta\rho}{\rho} = \frac{dg^3}{\gamma^2}\left(\frac{\varepsilon}{1-\varepsilon}\right)$$

for small values of ε the ratio $\varepsilon/(1-\varepsilon)$ can be approximated by ε.

Accordingly Eq. (1) leads to

$$K \propto \varepsilon^{0.33} \tag{2}$$

Previous studies on gas holdup (ε) [34] show that the gas holdup is related to the superficial gas velocity by the equation:

$$\varepsilon \propto V_g^n \tag{3}$$

In the bubbly flow regime n lies between 0.7 and 1.2 [34] i.e. $n \approx 1$. Eliminating ε between Eqs. (2) and (3) we get

$$K \propto V_g^{0.33} \tag{4}$$

(2) *The penetration model* [35]. This model is based on the fact that bubble detachment from the mercury surface creates a void which is filled with fresh solution through which unsteady state diffusion of the reactant to the mercury surface takes place until a new bubble is formed. A relation between the mass transfer coefficient at the gas evolving surface and the superficial gas velocity was obtained by Ibl and Venczel [35] by integrating the Cottrell equation over the waiting time t_w and taking the time average:

$$K = t_w^{-1}\int_0^{t_w}\left(\frac{D}{\pi t}\right)^{0.5} \mathrm{d}t \tag{5}$$

Assuming hemispherical bubbles, Ibl and Venczel calculated the waiting time t_w as the inverse of the number of bubbles evolved at a site per unit time:

$$t_w = \frac{(\pi d_b^3/6)A}{\pi r_b^2 V_g} \tag{6}$$

Using the above expression after taking into account that only a fraction θ of the electrode surface is covered by gas bubbles, Eq. (5) integrates to

$$K = \left[\frac{6DV_g(1-\theta)}{\pi_b A}\right]^{0.5} \tag{7}$$

Vogt [36] formulated the above equation in the following dimensionless form:

$$Sh = \frac{2.76}{\Phi^{0.33}}(Re\,Sc)^{0.5}(1-\theta)^{0.5} \tag{8}$$

where ϕ is a shape factor whose value depends on the bubble shape and θ the fractional surface coverage of the electrode by gas bubbles.

(3) *The microconvection model* [37]. This model is based on the fact that the growing bubble induces laminar flow past the transfer surface. Starting from the mass transfer equation which expresses the rate of mass transfer at a surface exposed to parallel laminar flow:

$$Sh = a\,Sc^{0.33}\,Re^{0.5} \tag{9}$$

Stephan and Vogt [37] could develop the following dimensionless equation which represents mass transfer at gas evolving surfaces:

$$Sh = 0.93\,Sc^{0.487}\,Re_g^{0.5} \tag{10}$$

The break off bubble diameter was used as a characteristic length in calculating *Sh* and *Re*. Both the penetration model and the microconvection model lead to:

$$K \propto V_g^{0.5} \tag{11}$$

Although Eqs. (8) and (10) are theoretically important, it is difficult to use them in practice to predict the rate of mass transfer at gas evolving surfaces owing to the difficulty of knowing bubble parameters such as break off bubble diameter, bubble geometrical parameter (ϕ) and fractional surface coverage (θ). This difficulty arises from the complex nature of electrical generation of gas bubbles where many interacting variables such as electrode material, solution composition nature of the evolving gas and the range of superficial gas velocity affect the process.

In view of this difficulty experimental studies such as the present one are necessary.

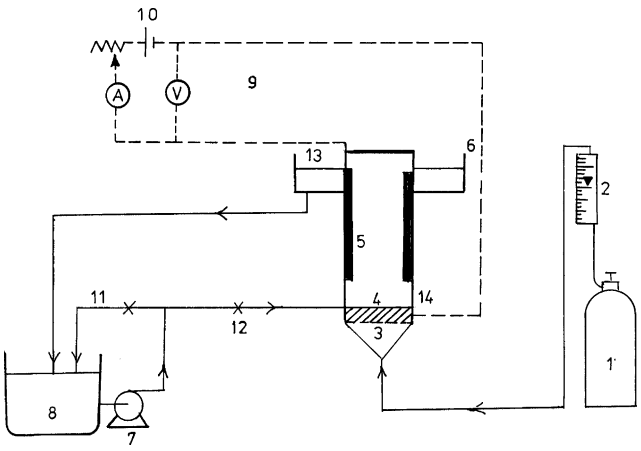

Fig. 1. Apparatus: (1) nitrogen cylinder, (2) rotameter, (3) sintered glass distributor, (4) mercury cathode, (5) stainless steel anode, (6) plexiglass overflow weir, (7) plastic centrifugal pump, (8) plexiglass storage tank, (9) electrical circuit (---), (10) 12 V dc power supply, (11) solution by pass, (12) plastic valve, (13) electrolyte level, (14) cylindrical plexiglass column.

3. Experimental technique

The apparatus (Fig. 1) consisted of the cell, flow-circuit and electrical circuit. The cell consisted of a plexiglass column of 11 cm diameter and 30 cm height, the bottom of the column was fitted with G4 sintered glass gas distributor. A layer of mercury of 1 cm height placed at the cell bottom formed the cathode, the anode was 25 cm high cylindrical screen of stainless steel liming the inner wall of the cell. The large anode area compared to the cathode area allowed the use of the anode as a reference electrode in constructing current–voltage curves from which the limiting current was obtained. The cathode and anode were fed with electrical current by nickel plated insulated copper wire. The electrical circuit consisted of 12 V dc power supply with a voltage regulator and a multirange ammeter connected in series with the cell. A voltmeter was connected in parallel. A 0.2 hp plastic centrifugal pump was used to circulate the electrolyte between 30 l plexiglass storage tank and the cell in experiments conduced to test the effect of single phase flow and the combined solution flow and gas sparging. Solution was admitted to the reactor from a side entry nozzle located at the mercury surface. Gas sparging was carried out using a N_2 cylinder and a calibrated rotameter to measure the superficial gas velocity.

Before each run, solution flow rate and or gas flow rate were adjusted at the required values by means of a bypass and ball valve, respectively. Solution velocity was determined by measuring the volume of solution collected in a certain time in a graduated cylinder. The limiting current of the cathodic reduction of ferricyanide ion which takes place according to the equation:

$$Fe(CN)_6^{3-} + e \rightarrow Fe(CN)_6^{4-}$$

was determined by increasing the current stepwise and measuring the corresponding cell voltage until the limiting current plateau was obtained.

The solution was composed of 0.01 M $K_3Fe(CN)_6$ and 0.01 M $K_4Fe(CN)_6$ in a large excess of NaOH, three different concentrations of NaOH were used: 1, 2 and 4 M. All solution were freed from dissolved oxygen by bubbling N_2 in the storage tank before and during experiments. Solution density and viscosity required for data correlation were determined by a density bottle and an Ostwald viscometer, respectively [38]. Diffusivity of ferricyanide ion was calculated from the equation [39–41]:

$$\frac{D\mu}{T}\,(\mathrm{kg\,m\,K^{-1}\,s^{-2}}) = 2.5 \times 10^{-15} \tag{12}$$

Temperature was measured during each run and the physical properties used in data correlation were adjusted accordingly. The present conditions provided *Sc* ranging from 1740 to 6000. Table 1 shows the physical properties of the solutions used at 25 °C. The limiting current was measured for three different hydrodynamic situations, namely: (i) batch gas sparged reactor; (ii) continuous gas sparged reactor with superimposed solution flow; (iii) continuous single phase flow reactor without gas sparging.

4. Results and discussion

Fig. 2a and b shows typical current–voltage curves for single phase flow and gas sparging, respectively, from which the limiting current was obtained, the mass transfer coefficient *K* was calculated from the limiting current under different conditions using the equation [41]:

$$K = \frac{1}{ZFAC} \tag{13}$$

Fig. 3 shows that the average *Sh* at a mercury pool whose surface is stirred by single phase flow from a side entry increases with the 0.89 power of *Re*, the smaller the feed nozzle diameter the higher the average *Sh*. The relatively high rate of mass transfer arises from the good mixing conditions

Table 1
Physical properties of the solutions at 25 °C

Solution composition	ρ (g/cm^3)	μ ($\times 10^2$ P)	D ($\times 10^6$ cm^2/s)	*Sc*
0.01 M $K_3Fe(CN)_6$ + 0.01 M $K_4FeCN)_6$ + 1 M NaOH	1.0461	1.1042	6.693	1577
0.01 M $K_3Fe(CN)_6$ + 0.01 M $K_4Fe(CN)_6$ + 2 M NaOH	1.085	1.3822	5.508	2314
0.01 M $K_3Fe(CN)_6$ + 0.01 M $K_4Fe(CN)_6$ + 4 M NaOH	1.1675	2.2743	3.291	5919

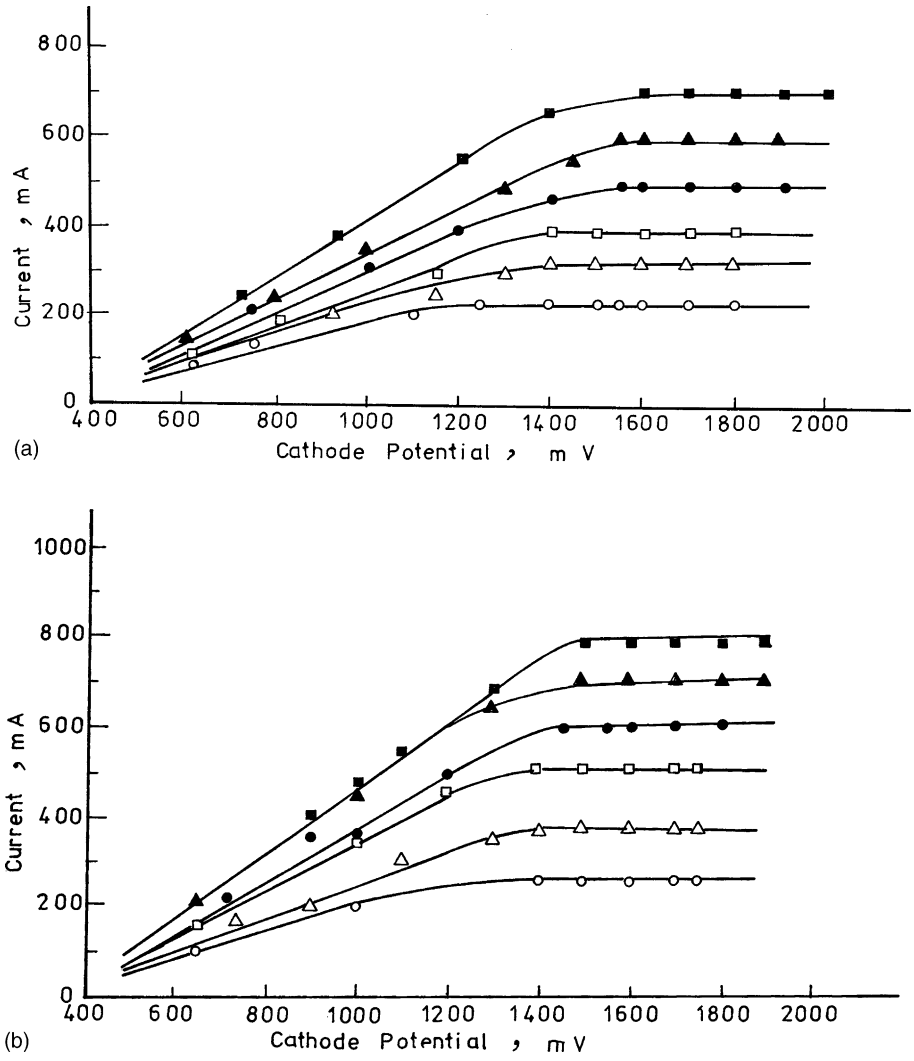

Fig. 2. (a) Typical current–voltage curves obtained for single phase flow at different solution velocities; $Sc = 2011$. Solution velocity in the reactor (V, cm/s): (○) 0.58, (△) 0.66, (□) 0.76, (●) 1.16, (▲) 1.35, (■) 1.9. (b) Typical current–voltage curves for gas sparged reactor at different superficial N_2 velocities ($V = 0$); $Sc = 1740$. Superficial N_2 velocity (V_g, cm/s): (○) 0.54, (△) 1.13, (□) 1.71, (●) 2.9, (▲) 3.53, (■) 4.17.

at the mercury surface as a result of exchange of momentum between the submerged horizontal jet and the surrounding solution, as the jet proceeds along the mercury surface it spreads widely to cover a large area of the mercury surface [42,43]. Fig. 4 shows that the mass transfer data for single phase flow under the conditions: $108 < Re < 5300$ and $5.5 < d/d_n < 22$ fit the equation:

$$Sh = 0.236\, Sc^{0.33}\, Re^{0.89} \left(\frac{d}{d_n}\right)^{0.68} \quad (14)$$

with an average deviation of +14%. Statistical analysis of the data has shown that the standard error is 2699, the 95% confidence limits are 3163 and 2235. Diameter of the mercury pool was arbitrarily used as a characteristic length in calculating Sh and Re. Based on inlet nozzle diameter Reynolds number, the above equation is valid for $594 < Re_n < 116\,600$. Since turbulent submerged jets prevails at $Re_n > 2000$ [44], it follows that most of the present data were obtained using turbulent submerged horizontal jets, this is consistent with high Re exponent (0.89) shown in Eq. (14).

Fig. 5 shows the effect of N_2 superficial velocity on the mass transfer coefficient in a batch reactor with no net solution flow, the mass transfer coefficient increases with increasing N_2 superficial velocity according to the equation:

$$K \propto V_g^{0.52} \quad (15)$$

The exponent 0.52 agrees with the values reported by previous experimental studies on mass transfer at gas evolving surfaces [36] and agrees with the value 0.5 predicted by the penetration model [35] and the microconvection model [37] which were presented to explain mass transfer at gas evolving electrodes. Visual observations of the mercury pool surface revealed that during gas sparging gas bubbles enveloped in a mercury film are formed on the mercury pool; after reaching a certain size where the buoyancy force is sufficient to overcome the surface tension force, the bub-

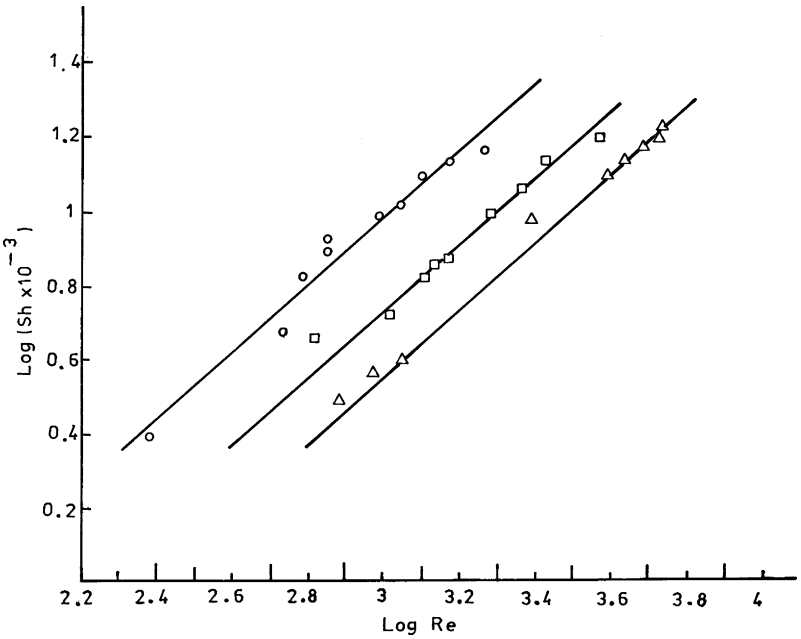

Fig. 3. log *Sh* vs. log *Re* at different distances using horizontal jet $Sc = 2011$. d_n (cm): (○) 0.5, (□) 1, (△) 2.

ble detaches from the surface of the mercury pool and its size increases suddenly owing to the change of the bubble envelope from mercury to water. The large bubble then disintegrates into small bubbles (the equilibrium size) at the mercury surface and then rise in the solution. The above events enhance the rate of mass transfer at the mercury surface via:

(i) Increasing the area of the mercury cathode through formation of N_2 bubbles with a mercury envelope at the mercury surface.
(ii) The sudden enlargement of the bubble leaving the mercury envelope induces radial momentum at the mercury surface.
(iii) The departure of the large bubbles from the mercury surface and the subsequent disintegration of these bubbles into small bubbles generate turbulence in the solution adjacent to the mercury surface.
(iv) The rise of bubbles in the solution induce a circulatory motion (backmixing) where the upward moving entrained solution is recycled downward at the container wall till it reaches the mercury surface.
(v) Bubble detachment from the mercury surface leads to vibrating the surface; Ross and Azim [45] who used the present technique to measure rates of mass transfer at mechanically vibrated mercury surface found that vibration increases the rate of mass transfer considerably.

An overall mass transfer correlation was envisaged in terms of the dimensionless groups *J*, *Re* and *Fr* usually used in correlating heat and mass transfer in gas sparged systems [25,26], Fig. 6 shows that the gas sparging mass transfer data

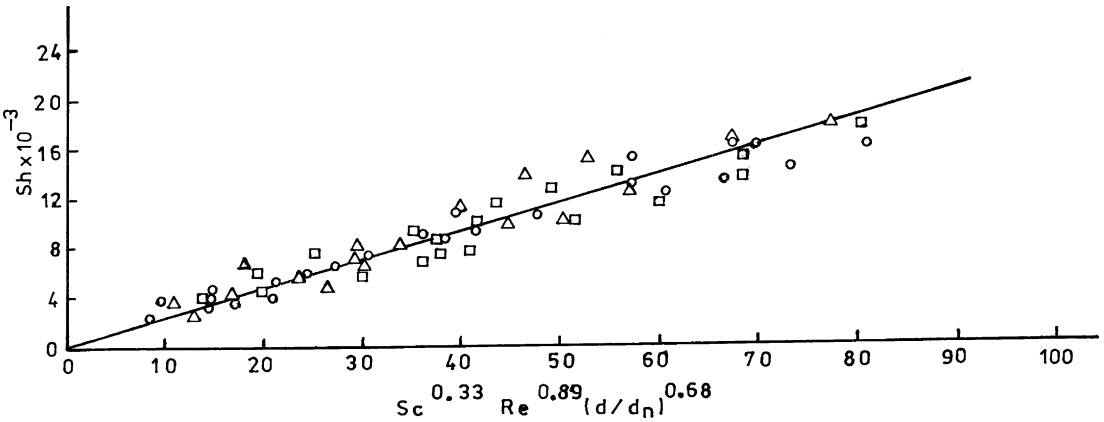

Fig. 4. Overall mass transfer correlation under single phase flow using horizontal jet. d_n (cm): (△) 0.5, (□) 1, (○) 2.

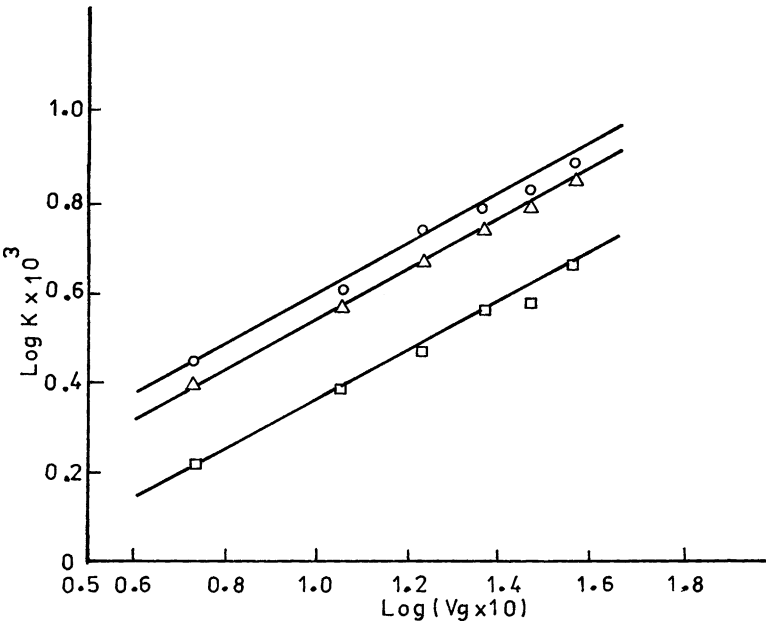

Fig. 5. Effect of superficial gas velocity on the mass transfer coefficient. *Sc*: (○) 1740, (△) 2565, (□) 6000.

in batch reactor for the conditions $0.046 < Re\,Fr < 10.1$ fit the equation:

$$J = 0.39(Re\,Fr)^{-0.16} \quad (16)$$

with an average deviation of +9.6%. The standard error is 0.054 and the 95% confidence limits are 0.039 and 0.069.

It would be instructive to compare the present gas sparging mass transfer data with previous related studies. Sedahmed and Ahmed [46] who studied the rate of mass transfer at H_2 evolving mercury cathode found that the mass transfer coefficient increases with the 0.27 power of H_2 discharge velocity. The difference between the present gas velocity exponent (0.52) and that obtained for H_2 evolving mercury cathode may be attributed to the difference in the mode of bubble generation at the mercury surface. Electrolytic H_2 generation at the mercury surface from alkaline solution produces small noncoalescing bubbles enveloped with aqueous film [47]. In the present study where gas comes from below the mercury surface, gas bubbles enveloped with mercury film are first formed at the mercury pool surface before they break off and turn into large gas bubbles enveloped with aqueous solution which disintegrate to the equilibrium sized bubbles. Events which are involved in the present mode of bubble generation such as enlargement of the mercury surface and turbulence generation by large bubble disintegration at the mercury surface may be responsible for the higher $\log K/\log V$ slope obtained in the present work compared to that obtained by Sedahmed and Ahmed.

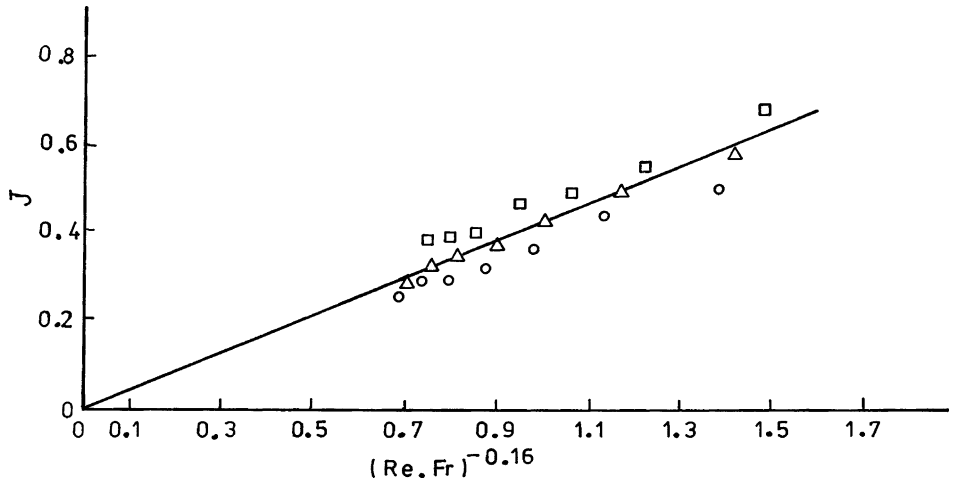

Fig. 6. Overall mass transfer correlation at gas sparged mercury cathode. *Sc*: (○) 1740, (△) 2565, (□) 6000.

In a previous study Sedahmed [26] derived the following equation which predict the rate of mass transfer at gas sparged solid surface by combining the surface renewal theory and Kolmogoroff's theory of isotropic turbulence:

$$St\,Sc^{0.5} = 0.035(Re\,Fr)^{-0.25} \quad (17)$$

By multiplying both sides by $Sc^{0.16}$ which for the present range of Sc approximates to 3.657, Eq. (17) becomes:

$$J = 0.128(Re\,Fr)^{-0.25}$$

A comparison between this equation and Eq. (16) shows that the present gas sparging mass transfer data are much higher than those predicted from Eq. (17). The high rate of mass transfer at the gas sparged mercury surface compared to that at a solid surface subjected to a swarm of gas bubbles generated by a porous frit is attributed to the fact that the intensity of turbulence generated at the immediate vicinity of the mercury surface during bubble growth and detachment is much higher than the intensity of turbulence (momentum) which is transferred from the rising gas–liquid dispersion to the solid transfer surface.

A model for heat transfer across liquid–liquid interfaces agitated by bubbles was developed by Szekely [48] using the surface renewal principles that assume periodic destruction of temperature gradients at the liquid–liquid interfaces by the arrival of bubbles. The model was further modified by Blottner [49] resulting in the following interfacial heat transfer coefficient:

$$h = 1.69\left(\frac{\rho C_p k V_g}{r_b}\right)^{0.5} \quad (18)$$

which can be written in the following dimensionless form:

$$Nu = 1.69\,Pr^{0.5}\,Re^{0.5} \quad (19)$$

bubble radius r_b was used as a characteristic length in calculating Re. The present result that the mass transfer coefficient increases with the 0.52 power of the superficial gas velocity is in agreement with Szekely's model. The criticism which can be levelled against Eq. (19) is that it needs a priori knowledge of the bubble radius which is not easy to determine beside the fact that it may not be uniform. Eq. (16) of the present work obviates this difficulty owing to the cancellation of the characteristic length from Eq. (16) ($Re\,Fr = V_g^3/Vg$). In applying Eq. (16) to predict the mass transfer coefficient in practice, care should be taken that the two liquid layers are completely separated and there is no entrainment of the lower liquid with the gas bubbles which try to pull in its wake a column of the heavier lower liquid into the light liquid layer. If the operating conditions allow entrainment to take place, Eq. (16) would be invalid owing to the increase in the rate of mass transfer as a result of the increase in the interfacial area between the two liquids. Greene [50] found that entrainment of the heavy liquid by the gas bubbles into the light liquid takes place when the bubble volume V_b exceeds a certain value given by

$$V_b > \left[\frac{7.8\sigma}{g(3\rho_1 - \rho_2 - 2\rho_g)}\right]^{3/2} \quad (20)$$

4.1. Mass transfer by the combined gas sparging and solution flow

To test the mass transfer behaviour of a continuous gas sparged mercury pool cathode, mass transfer rates were determined for the combined gas sparging and horizontal jet feed. To correlate the data the method used in correlating mass transfer data in cells with gas evolving electrodes and superimposed solution flow was invoked. Two models were developed in the literature to calculate the overall mass transfer coefficient at gas evolving electrodes with superimposed solution flow from the individual mass transfer coefficient due to gas evolution and forced convection. The first model simply adds the individual mass transfer coefficients [51]:

$$\bar{K} = K + K_g \quad (21)$$

The other one uses a vector addition [52–54]:

$$\bar{K} = (K^2 + K_g^2)^{0.5} \quad (22)$$

Under the present range of conditions it was found that the present data reasonably fit Eq. (22) while Eq. (21) overestimates the overall mass transfer coefficient. Table 1 shows that the overall mass transfer coefficient calculated from the gas sparging mass transfer coefficient and the single

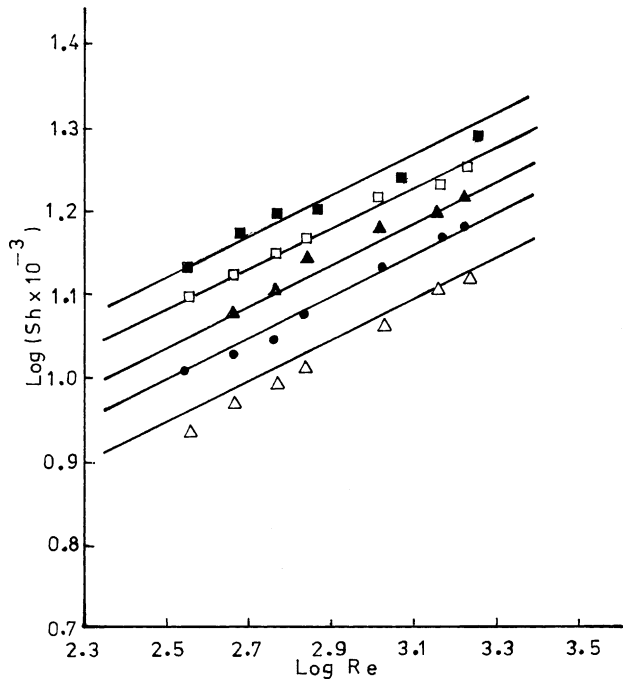

Fig. 7. Effect of solution Re on Sh at different superficial gas velocity (V_g, cm/s): (△) 0.54, (●) 1.71, (▲) 2.9, (□) 3.53, (■) 4.79.

Table 2
Comparison between the experimental overall mass transfer coefficient due to gas sparging and horizontal feed and the value calculated from Eq. (22)

V (cm/s)	V_g (cm/s)									
	1.13		1.7		2.3		3.53		4.8	
	$\bar{K}_{exp}$ ($\times 10^3$ cm/s)	$\bar{K}_{calc}$ ($\times 10^3$ cm/s)	$\bar{K}_{exp}$ ($\times 10^3$ cm/s)	$\bar{K}_{calc}$ ($\times 10^3$ cm/s)	$\bar{K}_{exp}$ ($\times 10^3$ cm/s)	$\bar{K}_{calc}$ ($\times 10^3$ cm/s)	$\bar{K}_{exp}$ ($\times 10^3$ cm/s)	$\bar{K}_{calc}$ ($\times 10^3$ cm/s)	$\bar{K}_{exp}$ ($\times 10^3$ cm/s)	$\bar{K}_{calc}$ ($\times 10^3$ cm/s)
0.26	5	4.24	5.34	5.61	6	6.14	7.1	7.74	8.18	8.83
0.48	5.45	4.5	6	5.8	6.55	6.32	7.74	7.9	8.73	8.96
0.58	6.5	4.74	7.1	6	7.6	6.5	8.45	8	9	9.08
0.67	7.14	5.33	7.6	6.5	8.18	6.94	9	8.4	9.8	9.4
0.76	7.6	5.9	7.9	6.95	8.18	7.39	9.27	8.76	10.1	9.74
1	8.2	6.7	9.8	7.6	9.81	8	12	9.3	12.8	10.22

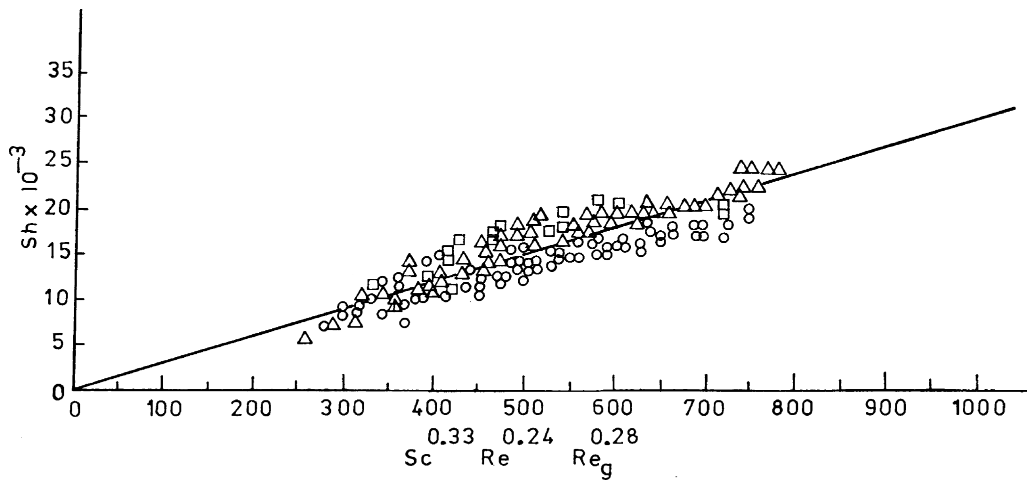

Fig. 8. Overall mass transfer correlation under two phase flow. Sc: (○) 1740, (△) 2565, (□) 6000.

phase mass transfer coefficient deviates from the experimental value by an average of +10.7%. Outside the range of conditions shown in Table 2 the deviation from Eq. (22) increases at lower gas velocities and higher solution velocities. The agreement of the present data with Eq. (22) implies that forced convection and gas evolution interact with each other at the mercury pool surface [52–54] probably as follows:

(i) Jet flow at the mercury surface contributes to the hydrodynamic conditions which affects the equilibrium bubble size at which the rate of coalescence becomes equal to the rate of disintegration [55].
(ii) On the other hand bubbles residing on the mercury surface may act as turbulence promoters for the jet flow.

In view of the fact that deviation from Eq. (22) becomes considerable at relatively low gas velocities and high solution velocities, an attempt was made to correlate all the mass transfer data obtained under the combined gas sparging and solution flow (typified by Fig. 7) in a manner similar to the used in case of two phase flow using the dimensionless groups Sh, Sc, Re and Re_g. Fig. 8 shows that the present data for the conditions $184 < Re < 1700$ and $338.5 < Re_g < 4747$ fit the equation:

$$Sh = 28\,Sc^{0.33}\,Re^{0.24}\,Re_g^{0.28} \quad (23)$$

with an average deviation of ±14%. The standard error is 2894 and the 95% confidence limits are 2546 and 3242. Mercury pool diameter was arbitrarily used as a characteristic length in calculating Sh, Re and Re_g.

5. Conclusion

(1) The present study have shown that gas sparging is an efficient means for enhancing the rate of diffusion controlled processes taking place at the interface between two immiscible nondispersed liquids such as purification and separation of organic melts by supercritical fluids, purification of molten metals by an overlying layer of slag, chemical and electrochemical processes involving the use of mercury pool. The increase in the rate of mass transfer ranged from 5 to 23 times the natural convection value depending on the operating conditions (the average natural convection mass transfer coefficient was found to be 0.55×10^{-3} cm/s).
(2) The present results show that mass transfer across a gas sparged interface between two immiscible liquids takes place through a mechanism similar to that of mass transfer at gas evolving surfaces, namely, by surface renewal

mechanism and/or microconvection mechanism which predict a dependence of the mass transfer coefficient on the 0.5 power of the gas velocity.

(3) The present dimensionless mass transfer correlations form the basis for the design and operation of a batch (simple or recirculating) and a continuous gas sparged mercury pool electrochemical reactor suitable for conducting small scale diffusion controlled organic and inorganic synthesis which cannot be conducted with other electrode material. The advantages of the continuous gas sparged mercury pool reactor is that it can be operated at low feed rate. The high residence time arising from the low feed rate and the high mass transfer coefficient resulting from gas sparging combine to increase the degree of conversion per pass. Besides, gas sparging would also assist in the continuous removal of any inert organic film which might foul the cathode surface during electrolysis.

References

[1] G.H. Sedahmed, M.S. Abdo, M.A. Kamal, O.A. Fadaly, H.M. Osman, Chem. Eng. Process. 40 (2001) 195.
[2] E.A. Soltan, S.A. Nosier, A.Y. Salem, I.A.S. Mansour, G.H. Sedahmed, Chem. Eng. J. 91 (2003) 33.
[3] M.M. Zaki, I. Nirdosh, G.H. Sedahmed, Can. J. Chem. Eng. 78 (2000) 1096.
[4] M.M. Zaki, I. Nirdosh, G.H. Sedahmed, Chem. Eng. Commun. 186 (2001) 43.
[5] G.V. Novakovic, N. Vunjak, L. Kundakovic, B. Obradovic, V. Nedovic, L. Sajc, B. Bugarski, Trends Chem. Eng. 5 (1998) 159.
[6] K. Schugerl, Chem. Eng. Sci. 52 (1997) 3661.
[7] Z.F. Cui, S. Chang, A.G. Fane, J. Membrane Sci. 221 (2003) 1.
[8] J.G. Khinast, A.A. Koynov, T.M. Leib, Chem. Eng. Sci. 59 (2003) 3961.
[9] S.Y. Lee, Y.P. Tsui, Chem. Eng. Prog. 95 (1999) 23.
[10] Y.T. Shah, Adv. Chem. Eng. 17 (1992) 1.
[11] M.P. Dudukovic, F. Larachi, P.L. Mills, Chem. Eng. Sci. 54 (1999) 1975.
[12] H. Vogt, Fortschr. Verfahrenstechnik 20 (1982) 269.
[13] M.A. Mc Hughand, V.T. Krukonis, Supercritical fluid extraction, Principle and Practice, 2nd ed., Butterworths, 1994.
[14] R. Parker, An Introduction to Chemical Metallurgy, 2nd ed., Pergamon Press, NY, 1978.
[15] M.C. Wilkinson, Chem. Rev. 72 (1972) 575.
[16] N. Glinka, General Chemistry, Mir, Moscow, 1970.
[17] W. Carruthers, Modern Methods of Organic Synthesis, 3rd ed., Cambridge University Press, Cambridge, UK, 1996.
[18] A.I. Vogel, A Text Book of Quantitative Inorganic Analysis, 5th ed., Longman, London, 1989.
[19] N.L. Weinberg, B.V. Tilak, Techniques of Electroorganic Synthesis, Wiley, NY, 1982.
[20] D.E. Danly, Emerging Opportunities for Electroorganic Processes—A Critical Evaluation of Plant Design and Economics, Marcel Dekker, 1984.
[21] S.G. Merica, N.J. Bunca, W. Jedral, J. Lipkowski, J. Appl. Electrochem. 28 (1998) 645.
[22] G. Pezzatini, S. Becagli, M. Innocenti, R. Guidelli, J. Electroanal. Chem. 444 (1998) 261.
[23] P.M. Roberston, B. Scholder, G. Thesis, N. Ibl, Chem. Ind. (1978) 459.
[24] K. Rajeshwar, J.G. Ibanez, Environmental Electrochemistry, Academic Press, NY, 1997.
[25] W.D. Deckwer, Chem. Eng. Sci. 35 (1980) 1341.
[26] G.H. Sedahmed, J. Appl. Electrochem. 15 (1985) 777.
[27] G.H. Sedahmed, A.Y. Hosny, O.A. Fadally, I.M. El-Mekkawy, J. Appl. Electrochem. 24 (1994) 139.
[28] O.N. Cavatorta, U. Bohm, Chem. Eng. Res. Des. 66 (1988) 265.
[29] N. Zuber, Int. J. Heat Mass Transfer 6 (1963) 53.
[30] L.J.J. Janssen, J.G. Hoogland, Electrochim. Acta 15 (1970) 1013.
[31] G.H. Sedahmed, L.W. Shemilt, J. Appl. Electrochem. 14 (1984) 123.
[32] G.H. Sedahmed, I. Nirdosh, Chem. Eng. Commun. 101 (1991) 93.
[33] E.J. Fenech, C.W. Tobias, Electrochim. Acta 2 (1960) 311.
[34] Y. Shah, B.G. Kelkar, S.P. Godbole, W.D. Deckwer, AIChE J. 28 (1982) 353.
[35] N. Ibl, J. Venczel, Metalloberflache 24 (1970) 365.
[36] H. Vogt, Gas evolving electrodes, in: E. Yeager, J.O.M. Bockris, B.E. Conway, S. Sarangapani (Eds.), Comprehensive Treatise of Electrochemistry, vol. 6, Plenum Press, NY, 1983.
[37] K. Stephan, H. Vogt, Electrochem. Acta 24 (1979) 11.
[38] A. Findly, J.K. Kitchner, Practical Physical Chemistry, Longman, London, 1960.
[39] J.R. Bourne, P. Dell'Ava, O. Dossenbach, T. Post, J. Chem. Eng. Data 30 (1985) 160.
[40] F. Berger, K.F. Hau, Int. J. Heat Mass Transfer 20 (1977) 1185.
[41] J.R. Selman, C.W. Tobias, Adv. Chem. Eng. 10 (1978) 211.
[42] M.R. Davis, H. Winarto, J. Fluid Mech. 101 (1980) 201.
[43] T. Maruyama, Y. Ban, T. Mizushina, J. Chem. Eng. Jpn. 15 (1980) 342.
[44] B.K. Revill, Jet mixing, in: N. Harnby, M.F. Edwards, A.W. Nieow (Eds.), Mixing in the Process Industries, 2nd ed., Butterworths/ Heinemann, Oxford, 1992.
[45] T.K. Ross, M.F. Azim, Chem. Eng. Sci. 26 (1971) 1771.
[46] G.H. Sedahmed, A.M. Ahmed, Can. J. Chem. Eng. 67 (1989) 942.
[47] L.J.J. Janssen, J.G. Hoogland, Electrochim. Acta 18 (1973) 543.
[48] J. Szekely, Int. J. Heat Mass Transfer 6 (1963) 417.
[49] Blottner, US Nucl. Regul. Comm. NUREG/CR-0944 (1979).
[50] G.A. Greene, Adv. Heat Transfer 21 (1991) 277.
[51] T.R. Beck, J. Electrochem. Soc. 116 (1969) 1038.
[52] H. Vogt, Electochim. Acta 32 (1987) 633.
[53] H. Vogt, Electrochim. Acta 23 (1978) 203.
[54] G. Bendrich, W. Seiler, H. Vogt, Int. J. Heat Mass Transfer 29 (1986) 1741.
[55] G. B. Wallis, One Dimensional Two Phase Flow, McGraw-Hill, NY, 1969.